Water Stress Explains the Aerodynamic versus Radiometric Surface Temperature Paradox in Thermal-based Evaporation Modeling

Kaniska Mallick[1*], Dennis Baldocchi[2], Andrew Jarvis[3], Tian Hu[1], Ivonne Trebs[1], Mauro Sulis[1], Nishan Bhattarai[4], Christian Bossung[1], Yomna Eid[5], Jamie Cleverly[6], Jason Beringer[7], William Woodgate[8,14], Richard Silberstein[9,15], Nina Hinko-Najera[10], Wayne S. Meyer[11], Darren Ghent[12], Zoltan Szantoi[13,16], Gilles Boulet[17], William P. Kustas[4]

[1]Department of Environmental Research and Innovation, Luxembourg Institute of Science and Technology, Belvaux, Luxembourg

[2]Department of Environmental Science Policy and Management, University of California, Berkeley, United States

[3]Lancaster Environment Centre, Lancaster University, Lancaster, UK

[4]Hydrology and Remote Sensing Laboratory, USDA-ARS, Beltsville, Maryland, United States

[5]The Julius Maximilians University of Würzburg, Wurzburg, Germany

[6]Terrestrial Ecosystem Research Network, College of Science and Engineering, James Cook University, Cairns, Queensland

[7]School of Agriculture and Environment, University of Western Australia, Crawley, WA, Australia

[8]School of Earth and Environment (SEE), The University of Western Australia, WA, 6009, Australia

[9]School of Science, Edith Cowan University, Joondalup, WA, Australia

[10]School of Ecosystem and Forest Sciences, The University of Melbourne, Creswick, Australia

[11]School of Biological Sciences, University of Adelaide, Adelaide, Australia

[12]University of Leicester, Department of Physics and Astronomy, Leicester, UK

[13]European Space Agency, Science, Applications & Climate Department, Frascati, Italy

[14]School of Earth and Environmental Sciences, The University of Queensland, QLD, 4072, Australia

[15]School of Agriculture and Environment, University of Western Australia, Crawley, WA, Australia

[16]Department of Geography & Environmental Studies, Stellenbosch University, South Africa

[17]Centre d'Etudes Spatiales de la Biosphère, Toulouse, France

[*]Corresponding author: Kaniska Mallick

email: kaniska.mallick@gmail.com, kaniska.mallick@list.lu

Key Points:

- Aerodynamic temperature and evaporation well estimated from physical principles and available energy-water limits over contrasting aridity
- Water stress predominantly influences the difference between aerodynamic and radiometric temperatures under sparse vegetation cover
- Analytical model offers an alternative parameter-sparse approach describing evaporation, canopy conductance and VPD interactions

Abstract

To explain the inequality between aerodynamic and radiometric surface temperature, we used an analytical surface energy balance model where evaporation is directly estimated by constraining the state equations of aerodynamic temperature and biophysical conductances through radiometric temperature. While the derived aerodynamic temperature was comparable with a flux-inverted counterpart, evaporation and sensible heat fluxes also showed good correspondence with in-situ eddy covariance observations over contrasting aridity in Australia. Results showed aerodynamic temperature frequently exceeds the radiometric temperature in arid and semiarid ecosystems for two reasons: (i) declining canopy-surface conductance and evaporative fraction due to escalated water stress and vapor pressure deficit, and (ii) a simultaneous increase in aerodynamic conductance, air temperature and sensible heat flux. The analytical approach provides valuable insights into the long-lasting debate of aerodynamic versus radiometric temperature paradox by recognizing the feedback between biophysical conductances and the supply-demand limit of solar radiation, soil moisture, and vapor pressure deficit.

Plain Language Summary

One of the longstanding research challenges in thermal remote sensing of evaporation is to resolve the incongruity between aerodynamic and radiometric surface temperature. Aerodynamic temperature drives the sensible heat flux from surface to atmosphere, and consequently affects evaporation through the surface energy balance. Yet, this temperature is an unobserved component in the surface energy balance models and is typically estimated from radiometric temperature using empirical parameterizations, which causes substantial uncertainty in evaporation estimates. Direct retrieval of this temperature will reduce uncertainties in global evaporation models. This study uses an analytical approach to directly retrieve the aerodynamic temperature and evaporation, based on the physical theory of surface energy balance without

involving any parameterizations of surface roughness and atmospheric stability. While comparison of the retrieved aerodynamic temperature with a locally derived counterpart indicated the role of empiricism in the aerodynamic conductance for causing their differences, evaporation and sensible heat fluxes compared reasonably well with observations across contrasting aridity and biomes. Overall, the results of this study demonstrate that the components of surface energy balance and associated state variables can be estimated from physical principles, offering an alternative and novel perspective to investigate the highly complex land-atmosphere interactions and feedback mechanisms.

1 Introduction

Radiometric surface temperature (T_r) obtained from thermal infrared (TIR) remote sensing is routinely used as a surrogate for aerodynamic temperature (T_0) in single-source surface energy balance (SEB) models for mapping evaporation (E) and sensible heat (H) fluxes (Kustas et al. 2007; Lhomme et al. 2000; Troufleau et al. 1997) However, the relationship between the two temperatures is both non-unique and poorly understood. While T_r corresponds to a weighted soil and canopy temperature as a function of radiometer view angle, T_0 represents an extrapolated air temperature at an 'effective depth' within the canopy at which the sensible heat flux arises (Boulet et al. 2012; Kustas et al. 2007). This depth is often referred to as the 'source-sink' height of the canopy at which T_r and T_0 can differ by several degrees. As a result, using them interchangeably may lead to large errors in evaporation estimates, particularly in arid and semiarid climates (Verhoef et al. 1997). The most common approaches adopted in the SEB models to accommodate the inequality between T_r and T_0 involve either empirical fitting parameters (e.g., kB^{-1}- extra resistance) (Boulet et al. 2012; Garratt and Hicks 1973; Lhomme et

al. 1997; Verma 1989) or contrasting parameterizations of biophysical conductances (Troufleau et al. 1997), which lack theoretical soundness.

Although a host of structurally different TIR-based models can reproduce the magnitude and variability in evaporation for a variety of ecosystems, many require parameter adjustments to reconcile with observations (Boulet et al. 2012; Li et al. 2019). This implies that there is still a major need to reduce the uncertain parameterizations in thermal evaporation modeling to describe such variations from the fundamental theoretical principles, which will provide methods to derive the environmental and biophysical impacts on global evaporation variability and ecosystem water use strategies. A fundamental challenge, however, is the non-linear dependency of evaporation not only on the environmental variables (e.g., radiation, temperature, humidity, wind speed, and soil moisture availability) but also on the biophysical states like aerodynamic and canopy-surface conductance, T_0, and vapor pressure. One approach to address this challenge is to use analytical modeling principles to constrain the magnitude and variability of these biophysical states and simultaneously estimate evaporation.

To constrain evaporation and understand the differences between the aerodynamic versus radiometric temperature using an analytical approach, we perceive the vegetation-atmosphere system as a box and consider the SEB fluxes as both the driver and driven by these biophysical states in the vegetation-atmosphere system. Assuming the surface-atmosphere exchange inside the box is operated within the available environmental and water limits, we can constrain the biophysical states by finding their analytical solution from the known boundary conditions of the box i.e., radiation, air temperature, humidity and T_r. This yields an analytical formulation of the SEB. Such an analytical formulation, called Surface Temperature Initiated Closure (STIC) has been shown to provide reasonable estimates of the evaporative fluxes across contrasting biomes

and aridity in the northern and southern hemisphere (Bai et al. 2021; Bhattarai et al. 2018; Bhattarai et al. 2019; Mallick et al. 2014; Mallick et al. 2018a; Mallick et al. 2016; Trebs et al. 2021). Additionally, the conductances showed specific sensitivities to radiation and water limitations (Mallick et al. 2018b; Trebs et al. 2021).

Here, we employ this analytical approach to gain insights into the physical connection between T_0 and T_r, and to understand the influence of the interactions between evaporation and conductances on controlling their differences. We used meteorological and SEB observations at eight eddy covariance sites from different ecological transects in Australia representing three different aridity classes and biomes. We also used remote sensing-based T_r in conjunction with observed solar radiation (R_G), air temperature (T_a), humidity (rH) as the main forcings and predicted the T_0, which was compared with a flux-inverted reference value. We evaluated T_0 and analyzed its difference to T_r across a range of aridity conditions using data of eight years. We subsequently investigated the extent to which the response of canopy-surface conductance to soil water content and vapor pressure deficit alters the differences between T_0 and T_r, and evaluated the performance of the analytical solution of T_0 and conductances to derive evaporation and H. Section 2 provides a brief description of the analytical model, remote sensing data, and the observations used at the eight Australian sites. Section 3 focuses on analyzing the predicted T_0 with respect to a local T_0 and in-situ T_r, and assessing the role of radiative energy and available water on their differences. The effects of interactions between the biophysical conductances, vapor pressure deficit, temperature and surface energy balance observations are subsequently investigated to understand the paradox of T_r versus T_0. We conclude with an outlook on a potential step forward for rethinking and simplifying thermal evaporation models and the utility

of the analytical approach to study water stress induced effects on evaporation and land-atmosphere interactions.

2 Methods and data

2.1 Model based retrieval of T_0

For retrieving T_0, we used the non-parametric yet physically based Surface Temperature Initiated Closure (STIC) model (Mallick et al., 2018; Trebs et al., 2021; Bhattarai et al., 2018). STIC is based on integration of T_r information into the Penman–Monteith Energy Balance (PMEB) equation (Monteith, 1965). One of the fundamental assumptions in STIC is the first order dependence of T_0, aerodynamic and canopy-surface conductance (g_a and g_{cs}) on an aggregated moisture availability index (I_{SM}), which is retrieved through T_r. In STIC, the vegetation–substrate complex is considered as a single slab and it hypothesizes that T_0 is the temperature to which the stomatal and non-stomatal elements of canopy-air space respond.

By integrating T_r with standard SEB theory and vegetation biophysical principles, STIC formulates multiple state equations of T_0, g_a, g_{cs} to eliminate the need of using any empirical parameterizations of these variables. The state equations are connected with T_r through I_{SM}, and the effects of T_r are subsequently propagated into their analytical solutions. The equations are based on the aerodynamic bulk transfer hypothesis, advection-aridity hypothesis (Brutsaert and Stricker 1979), and evaporative fraction (F_E) theory (Shuttleworth et al. 1989; Mallick et al. 2016). Their detailed derivations are provided in S1 of the supporting information.

$$g_a = \frac{R_N - G}{\rho c_p \left[(T_0 - T_a) + \frac{(e_0 - e_a)}{\gamma} \right]} \quad (1)$$

$$g_{cs} = g_a \frac{(e_0 - e_a)}{(e_0^* - e_0)} \quad (2)$$

$$T_0 = T_a + \frac{(e_0 - e_a)}{\gamma}\frac{(1 - F_E)}{F_E} \quad (3)$$

$$F_E = \frac{2\alpha s}{2s + 2\gamma + \gamma(1 + I_{SM})\frac{g_a}{g_{cs}}} \quad (4)$$

R_N and G are net radiation and ground heat flux (W/m^2), e_0^* and e_0 are the saturation vapor pressure and ambient vapor pressure at the source-sink height (hPa), e_a is the atmospheric vapor pressure (hPa) at the level of T_a measurement, ρ is the air density (kg/m3), c_p is the specific heat of air at constant pressure (j/kg/K), γ is the psychrometric constant (hPa/°C), *s* is the slope of the saturation vapor pressure at T_a (hPa/°C), and α is the Priestley-Taylor coefficient (Priestley and Taylor, 1972), respectively. The inputs needed for computation of T_0, conductances and SEB fluxes through STIC are T_a, T_r, relative humidity (rH) or e_a, downwelling and reflected global radiation (R_G and R_r). Estimation of R_N follows the method of Bhattarai et al. (2018) and G follows Santanello and Friedl (2003) where the original method is modified by introducing I_{SM} in the G formulation (details provided in S1 of the supporting information.). Given the estimates of I_{SM}, R_N, G, the four state equations can be solved simultaneously to derive their analytical solutions. However, the analytical expressions contain three accompanying unknowns; e_0, e_0^*, and □. Therefore, an iterative solution was needed to determine the three unknown variables. Once the analytical solutions of g_a and g_{cs} are obtained, both variables are returned into the PMEB equation to directly estimate E.

I_{SM} is a unitless quantity, which describes the relative wetness of the surface and it controls the transition from potential to actual evaporation; which implies $I_{SM} \rightarrow 1$ under saturated surface and $I_{SM} \rightarrow 0$ under dry surface. Therefore, I_{SM} is critical for providing a constraint against which the T_0 and conductances are estimated. Since T_r is extremely sensitive to the surface moisture variations, it is extensively used for estimating I_{SM} in a physical retrieval scheme (Bhattarai et

al., 2018; Mallick et al., 2016, 2018a). In STIC, I_{SM} is expressed as a function of the dewpoint temperature difference between the source-sink height and air to T_r and air dewpoint temperature difference and the details of I_{SM} estimation are provided in S1 of the supporting information. In STIC, an initial value of α was assigned as 1.26; initial estimates of e_0^* were obtained from T_r through temperature-saturation vapour pressure relationship, and initial estimates of e_0 were obtained from I_{SM} as $e_0 = e_a + I_{SM}(e_0^* - e_a)$. Initial T_{0D} and I_{SM} are estimated according to Venturini et al. (2008) (detail in S1 supporting information), and initial estimation of G was performed from R_N and initial I_{SM} (detail in S1 supporting information). With the initial estimates of these variables; first estimates of the conductances, T_0, F_E, H, and E were obtained. The process was then iterated by updating e_0^*, e_0, T_{0D}, I_{SM}, and α (using eq. A9, A10, A11, A17, A16 and A15 in Mallick et al., 2016), with the first estimates of g_{cs}, g_a, T_0, and E, which was followed by re-computing G, g_{cs}, g_a, T_0, F_E, H, and E in the subsequent iterations with the previous estimates of e_0^*, e_0, T_{0D}, I_{SM}, and α until the convergence of E was achieved. Stable values of E are obtained within ~10-15 iterations.

2.2 Datasets and study sites

We used in-situ and remote sensing observations for model simulation and analysis. Level 3 post-processed and gap-filled meteorological, soil moisture, and SEB flux observations from the Australian eddy covariance (EC) flux tower network OzFlux (http://data.ozflux.org.au/portal/home.jspx) (Beringer et al. 2016) is used. SEB fluxes, conductances, and T_0 were simulated for the years 2011–2018 for eight OzFlux sites distributed in different ecological transects in Australia. The sites represent three broad ecological habitats namely arid, semiarid and mesic, covering a broad range of climate and ecosystem types (Table 1).

Daily clear-sky T_r observations from MODIS onboard Terra and Aqua at 1 km spatial resolution were obtained from the European Space Agency, Climate Change Initiative (ESA CCI+) land surface temperature (LST) consortium (Ghent et al. 2019) for the corresponding tower pixels using their location information (Table 1). In addition, the MODIS Terra-Aqua combined 4-day LAI (MCD15A2Hv006) product with a spatial resolution of 500 m was used for estimating the fractional vegetation cover (f_v).

Table 1: An overview of general characteristics of the measurement sites of the OzFlux network used in this study as reported in Trebs et al. (2021). Model simulations were made for the period 2011–2018 (except GWW 2013–2018).

Aridity	Ecological transect	Site name	Lat/ Lon	P (±□) (mm)	Mean aridity index (range)	World ecoregion	LAI range	Source-sink height (m)
Arid	NATT	Alice Springs Mulga (ASM)	-22.2828 / 133.2493	302 (61)	31 (6 - 133)	Deserts and xeric shrublands	0.16 - 0.85	4.9
	TREND	Calperum (CPR)	-34.0027 / 140.5877	207 (66)	21 (8 - 40)	Mediterranean woodlands	0.17 - 0.66	2.1
	SWATT	Great Western Woodlands (GWW)	-30.1913 / 120.6541	283 (52)	11 (5 - 22)	Mediterranean woodlands	0.29 - 0.49	11
Semiarid	SWATT	Gingin (Gin)	-31.3764 / 115.7139	560 (44)	8 (4 - 22)	Mediterranean woodlands	0.58 - 1.27	4.78
	NATT	Sturt Plains (Stp)	-17.1507 / 133.3502	581 (48)	7 (2 - 26)	Tropical grasslands	0.15 - 1.35	0.39
	NATT	Dry River (Dry)	-15.2588 / 132.3706	708 (43)	6 (2 - 12)	Tropical savannas	0.7 - 2.0	8.58
Mesic	TREND	Wombat (Wom)	-37.4222 / 144.0944	1116 (34)	4 (3 - 10)	Tropical savannas	2.2 - 4.9	16.3
	BATS	Tumbarumba (Tum)	-35.6566 / 148.1517	1400 (46)	1.6 (0.8 - 2)	Temperate broadleaf and mixed forest	1.0 - 3.4	31.2

P = mean annual precipitation; LAI = leaf area index; Source-sink height was calculated from the Table 3 of Trebs et al. (2021) as z_{0m} + d where z_{0m} is the roughness length for momentum transfer and d is the displacement height.
NATT: North Australian Tropical Transect; SWATT: South West Australian Transitional Transect; TREND: TRansect for ENvironmental Monitoring and Decision Making; BATS: Biodiversity and Adaptation Transect Sydney

198 2.3 Data analysis

199 Since MODIS T_r was used to retrieve STIC T_0, their relationship and differences were analyzed
200 in light of satellite view zenith angle (vza), R_G, soil water content (SWC) and vegetation cover
201 (f_v) limits. Additional analysis and verification was also done by comparing in-situ T_r with a
202 reference T_0 derived from EC (inverted T_0, hereafter) (details in S2 of SI).

203 Inverted T_0 estimation requires information about R_G, R_r, T_a, T_r, and the value of g_a, g_{cs},
204 respectively. For the first three variables, we directly use the observations. In-situ T_r was
205 estimated from the observations of upwelling and downwelling longwave radiation and surface
206 emissivity using the expression from Wang et al. (2005) (details in S2). In-situ g_a was estimated
207 from direct observations of wind speed (u) and friction velocity (u^*). In-situ g_{cs} was estimated
208 from R_N, G, atmospheric vapor pressure deficit (D_a) observations and g_a. A detailed description
209 of the estimation of individual variables is provided in S2 of SI.

210 **3 Results and discussion**

211 STIC and inverted T_0 estimates were significantly correlated ($r = 0.84 - 0.96$, $p<0.05$) (Fig. 1a -
212 c) for the observed range of H. However, the scatterplots revealed unequal variability of the two
213 temperatures, particularly in arid and semiarid ecosystems. The mean bias and root mean square
214 difference (RMSD) between the two temperatures were about -0.73 to 3.26°C and 2.57 to
215 5.50°C, with systematic RMSD of 35-43%. The residual difference between STIC versus
216 inverted T_0 appeared to be robustly related to tower-based g_a estimates ($r = 0.42 - 0.87$, $p<0.05$)
217 (inset of Fig. 1a-c). This implies that assuming a constant inverse Stanton number ($kB^{-1} = 2$) in
218 the numerator of equation S2.9 does not adequately capture the expected variations in flux-
219 inverted T_0. Additionally, the range of errors associated with MODIS T_r could be partly
220 responsible for the differences between STIC T_0 and inverted T_0.

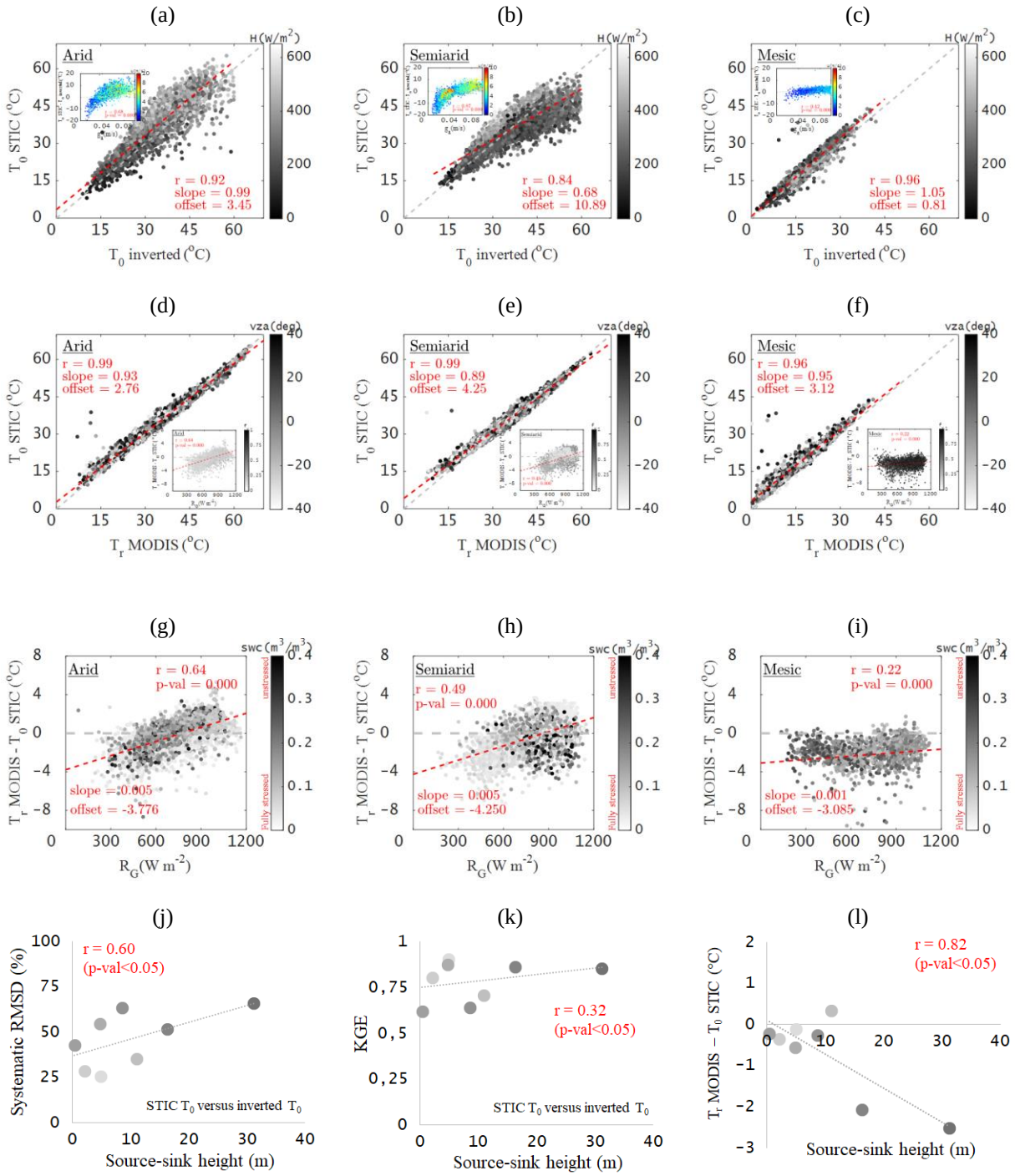

Figure 1. (a)-(c) Comparison between STIC T_0 versus inverted T_0 by combining data of all arid, semiarid, and mesic sites. The figures in the inset show how the differences between T_0 estimates depend on tower-derived aerodynamic conductance (g_a). (d)-(f) Comparison between STIC T_0 and in-situ T_r by combining data of all the arid, semiarid, and mesic sites. The figures in the inset show the relationship between T_r-T_0 differences with shortwave radiation (R_G) for a wide range of fractional vegetation cover (f_v). (g)-(i) Scatterplot showing the relationship between T_r-T_0 differences with R_G for a wide range of soil water content (SWC) representing fully stressed to unstressed conditions. (j)-(l) Scatterplot showing the systematic root mean square difference (RMSD) and Kling Gupta Efficiency (KGE) between the two T_0 estimates and the difference between T_r versus T_0 was significantly correlated with the source-sink height.

Comparison of STIC T_0 with MODIS T_r revealed T_0 differed from T_r by ±4-6°C in arid and semiarid ecosystems and T_0 consistently exceeded T_r in the mesic ecosystems. While their relationship (r = 0.96 - 0.99, slope = 0.89 - 0.95, intercept = 2.76 - 4.25) was independent of satellite view zenith angle (vza) variations (Fig. 1d-f), T_r-T_0 was significantly correlated with R_G and H for the entire range of fractional vegetation cover (f_v) and soil water content (SWC) in all the ecosystems (r = 0.22 - 0.64, p<0.05) (inset Fig. 1d-f, Fig. 1g-h, Fig. S2 in SI). In arid and semiarid ecosystems, T_r-T_0 increased with increasing R_G, and T_0 increasingly exceeded T_r with declining SWC at constant R_G when the magnitude of R_G was high (>600 W m^{-2}). No distinct pattern between T_r-T_0 and R_G was found in the mesic ecosystems (Fig 1i). A comparison between the inverted T_0 and in-situ T_r revealed the similar pattern as found in Fig. 1d-i (Fig. S3 in SI).

The statistical errors (RMSD and Kling Gupta Efficiency, KGE) between STIC versus inverted T_0 and the mean difference between MODIS T_r and STIC T_0 was significantly correlated with the 'source-sink' height (r = 0.32 - 0.82, p<0.05; Fig. 1j - l). Nevertheless, results indicate that T_0 is retrievable with the analytical approach and Figure 2 (below) discusses the reasons for T_0 versus T_r inequality based on the interactions of STIC derived conductances with SEB observations under different soil water stress.

Depending on aridity and vegetation characteristics, evaporation response to increasing vapor pressure deficit (D_a) varies from strongly decreasing to increasing (Massmann et al. 2019). The present study revealed two distinct patterns of T_r-T_0 depending on canopy-surface conductance (g_{cs}) and evaporative fraction (F_E) responses to D_a and vegetation characteristics. In arid and semiarid ecosystems, sparse vegetation in conjunction with high D_a, radiative heating, and water stress triggers a decline in g_{cs} (Grossiord et al. 2020), F_E and humidity at the source-sink height

(Fig. S4 in SI). This leads to a substantial increase in vapor pressure deficit at the source-sink height (D_0) ($D_0 >> D_a$). A cascade of subsequent impacts followed an increase in H, T_a, and g_a at the cost of a decline in F_E and the g_{cs}/g_a ratio due to high D_0 - D_a (Fig 2a-b; 2d-e). The scatterplot of H versus F_E for a range of g_{cs}/g_a showed that while H increases with decreasing g_{cs}/g_a at a constant F_E, H also increases with declining F_E for a constant g_{cs}/g_a (Fig. 2d-e). For a constant dT_r, H increases with increasing g_a; and for a constant H, dT_r increases with decreasing g_a. However, when both g_a and H vary together, dT_r decreases with increasing H and g_a (inset of Fig. 2d-e). While high g_a leads to high H at the cost of reduced F_E and g_{cs}, close vegetation-atmospheric coupling, rising soil water stress, and high D_0 leads to an escalation of T_0 beyond T_r (Fig. 2g-h). However, for sparse vegetation, when soil temperature is higher than the vegetation temperature due to high water stress, T_r exceeds T_0 due to the larger impact of soil temperature on T_r (Boulet et al. 2012; Huband and Monteith 1986). In mesic ecosystems with high SWC, consistently lower T_r than T_0 was due to high evaporative cooling from the transpiring vegetation (Lin et al. 2017).

Figure 2 (j-l) compares the evaporation (E) (as latent heat fluxes) and H derived from STIC with observations, showing good agreement with regression coefficients of 0.70 - 0.91 for H and a slightly lower correlation for E (0.51 - 0.70). One of the major factors shaping evaporation in radiation-controlled (mesic) and water-controlled (arid and semiarid) ecosystems is soil water availability, and STIC clearly distinguished the water stress impacts on evaporation. Water stress mainly affects g_{cs} to reduce evaporation, which is reasonably captured by the analytical model. Interestingly, the substantial difference in surface roughness between these ecosystems apparently had little effect on E and H retrieval through STIC.

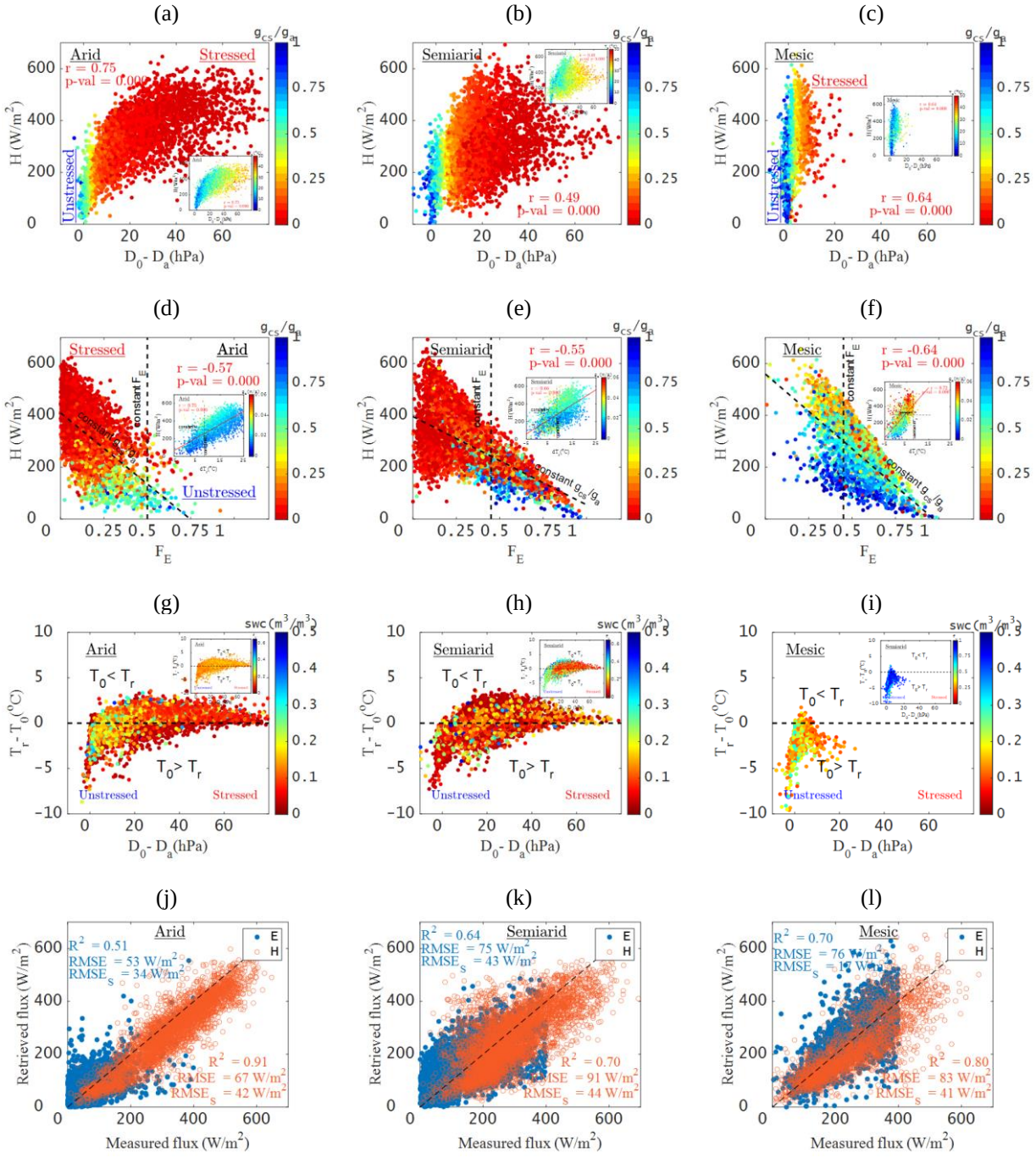

Figure 2. Scatterplots showing how the increase in source-sink height vapor pressure deficit (D_0) and its departure from D_a leads to a decline in g_{cs}/g_a ratio and evaporative fraction at the cost of increasing the H and T_a (a-b, d-e). Under low to moderate fractional vegetation cover, elevated water stress and high H leads to increased T_0 and D_0 at the source-sink height (g-h), thus increasing T_0 beyond T_r. (j-l) Retrieved versus measured E and H by combining data of all sites in an individual aridity class.

Some limitations of our approach are worth mentioning. First, our approach does not explicitly consider atmospheric stability. However, we anticipate such effects are embedded in the dT_r.

Second, it relies on an aggregated water stress factor to derive lumped estimates of canopy-surface conductance. Retrieving a pure canopy-stomatal conductance signal needs an explicit description of soil-canopy energy balance, which tends to shed more light on this analysis. This needs more work, and it is beyond the scope of the present study. Yet, the highly explained variance of the T_0 and conductances from mid-morning and afternoon hours suggests that the analytical approach captures the fundamental biophysical factors that shape up the SEB fluxes, thereby providing relevant insights into thermal-based evaporation modeling and land-atmosphere interactions across a large spectrum of biomes and climates.

TIR-based evaporation retrievals have been validated over the last decades using several structurally different models with diverse soil-canopy conductance parameterizations (Boulet et al. 2012; Kustas and Anderson 2009). Some studies also emphasized the pivotal role of T_0 estimation and concluded that empirical parameterizations and adjustments of the conductances to accommodate the inequality between T_0 and T_r are not appropriate to estimate evaporation over sparse canopies (Lhomme et al. 1997; Troufleau et al. 1997). These parameterizations are not stationary and vary with vegetation structure, water stress and climatic conditions, and they should therefore be used with caution before being used in an operational manner (Bhattarai et al. 2018; Kustas et al. 2007; Trebs et al. 2021; Verhoef et al. 1997). We advance the understanding of land surface processes by showing that the differences between T_0 and T_r is primarily shaped by water stress induced variations in canopy-surface conductance and evaporation in arid and semiarid ecosystems, along with their subsequent influence on sensible heat flux, air temperature and aerodynamic conductance. STIC reproduces the variability in T_0, conductances, and evaporation across the seasons and over highly contrasting climate and biomes. It is somewhat remarkable that H was relatively less dynamic as compared to

evaporation across different ecosystems, despite contrasting water availability and surface roughness. This indicates that surface roughness is also likely to play a significant role in shaping the interactions between the T_0 and conductances. Such interactions are likely to be reproduced in STIC, despite being independent of any surface roughness parameterization. This suggests that from the reliable information of available energy and water stress limits, it is possible to understand the differences between T_0 and T_r while simplifying the complexities in TIR-based evaporation modeling. The analytical framework of STIC sets the available energy and water limits through T_r, which is why the interactions between conductances, evaporation and T_0 are explained without the need for knowing wind speed information or applying corrections for atmospheric stability.

4 Conclusions

We showed that the aerodynamic versus radiometric surface temperature paradox can be explained across different types of climate and ecosystems using the analytical surface energy balance framework of STIC. This provides novel, non-parametric means to retrieve evaporation and opens perspective to further investigate the effects of water stress on canopy conductance and global evaporation variability. The framework is set by algebraic reorganization of bulk-transfer equations and a coupled net available energy formulation constrained by radiometric surface temperature variations, which leads to the analytical solutions of aerodynamic temperature and biophysical conductances. Results show that the differences between aerodynamic and radiometric temperature occur due to constrained evaporation triggered by soil water stress and rising atmospheric water deficits at the arid and semiarid ecosystems, and due to evaporation induced cooling in mesic ecosystems. Comparison of modeled versus observed evaporation and sensible heat flux suggests that the surface energy balance components can be

315 constrained with radiometric surface temperature for all ranges of vegetation cover and water
316 availability, without any need of specifying explicitly an aerodynamic surface roughness
317 function.

318 We conclude that our approach represents an appropriate basis to understand the differences
319 between long debated aerodynamic (T_0) versus radiometric surface temperature (T_r). It gives a
320 novel perspective and motivates the need to understand temperature-evaporation interactions
321 from the first principles and how such interactions are driven by (and drives) the biophysical
322 variables in a broad range of water and radiation-controlled environments. These interactions are
323 reflected in STIC at the fundamental level and our study indicated the potential role of
324 biophysical homoeostasis. The homoeostasis of T_r is evidenced by a coordinated response of the
325 canopy-surface conductance to vapor pressure deficit during high soil water stress and radiative
326 heating of the canopy. The inequality between T_0 and T_r is likely to have evolved largely as a
327 consequence of homoeostasis for a given fractional canopy cover and surface to root zone water
328 stress. The reshaping of T_r due to homoeostasis is a thermoregulation of vegetation for surviving
329 in water-scarce environments. This leads to the self-organization of vegetation, yet the
330 magnitude of T_r is well constrained by relative apportioning of evaporation and sensible heat
331 fluxes. This self-organization then affects the biophysical conductances quite substantially.
332 Consequently, our results indicate that T_0 versus T_r inequality is powered by the interaction
333 between biophysical conductance and the supply-demand limit of solar radiation, soil water
334 stress and vapor pressure deficit.

335 **Acknowledgments**

336 KM acknowledges the funding from ESA CCI+ Phase1 New ECVS LST (ESA/Contract No.
337 400123553/18/I-NB) and Mobility Fellowship from the FNR Luxembourg

(INTER/MOBILITY/2020/14521920/MONASTIC). MS acknowledges financial support from the financial support of the FNR CORE programme (CAPACITY, C19/SR/13652816). The OzFlux and Supersite network is supported by the National Collaborative Infrastructure Strategy (NCRIS) through the Terrestrial Ecosystem Research Network (TERN). WW is supported by an Australian Research Council DECRA Fellowship (DE190101182). Mention of trade of names or commercial products in this publication is solely for the purpose of providing specific information and does not imply recommendation or endorsement by the U.S. Department of Agriculture. USDA is an equal opportunity provider and employer.

Open research

The MODIS Terra and Aqua land surface temperature data are available through https://gws-access.jasmin.ac.uk/public/esacci_lst/LIST/. Level-3 eddy covariance data in netcdf format over the Ozflux sites are available from https://data.ozflux.org.au/portal/pub/viewColDetails.jspx?collection.id=152&collection.owner.id=101&viewType=anonymous (ASM), https://data.ozflux.org.au/portal/pub/viewColDetails.jspx?collection.id=1882712&collection.owner.id=703&viewType=anonymous (CPR), https://data.ozflux.org.au/portal/pub/viewColDetails.jspx?collection.id=750&collection.owner.id=503&viewType=anonymous (GWW), https://data.ozflux.org.au/portal/pub/viewColDetails.jspx?collection.id=1883250&collection.owner.id=768&viewType=anonymous (Gin), https://data.ozflux.org.au/portal/pub/viewColDetails.jspx?collection.id=1882702&collection.owner.id=304&viewType=anonymous (Dry), https://data.ozflux.org.au/portal/pub/viewColDetails.jspx?collection.id=1882705&collection.ow

ner.id=304&viewType=anonymous (Stp),

https://data.ozflux.org.au/portal/pub/viewColDetails.jspx?collection.id=1882717&collection.ow

ner.id=2022264&viewType=anonymous (Tum), and

https://data.ozflux.org.au/portal/pub/viewColDetails.jspx?collection.id=1882713&collection.ow

ner.id=2021351&viewType=anonymous (Wom), respectively. Archiving of the harmonized time series datasets over the study grids is being underway and will be available in Zenodo.org upon the acceptance of the manuscript. Codes of the analysis are available to the first author upon reasonable request.

References

Bai, Y., Zhang, S., Bhattarai, N., Mallick, K., Liu, Q., Tang, L., Im, J., Guo, L., & Zhang, J. (2021). On the use of machine learning based ensemble approaches to improve evapotranspiration estimates from croplands across a wide environmental gradient. *Agricultural and Forest Meteorology, 298*, 108308

Beringer, J., Hutley, L.B., McHugh, I., Arndt, S.K., Campbell, D., Cleugh, H.A., Cleverly, J., Resco de Dios, V., Eamus, D., & Evans, B. (2016). An introduction to the Australian and New Zealand flux tower network–OzFlux. *Biogeosciences, 13*, 5895-5916

Bhattarai, N., Mallick, K., Brunsell, N.A., Sun, G., & Jain, M. (2018). Regional evapotranspiration from an image-based implementation of the Surface Temperature Initiated Closure (STIC1. 2) model and its validation across an aridity gradient in the conterminous US. *Hydrology and Earth System Sciences, 22*, 2311-2341

Bhattarai, N., Mallick, K., Stuart, J., Vishwakarma, B.D., Niraula, R., Sen, S., & Jain, M. (2019). An automated multi-model evapotranspiration mapping framework using remotely sensed and reanalysis data. *Remote Sensing of Environment, 229*, 69-92

Boulet, G., Olioso, A., Ceschia, E., Marloie, O., Coudert, B., Rivalland, V., Chirouze, J., & Chehbouni, G. (2012). An empirical expression to relate aerodynamic and surface temperatures for use within single-source energy balance models. *Agricultural and Forest Meteorology, 161*, 148-155

Brutsaert, W., & Stricker, H. (1979). An advection-aridity approach to estimate actual regional evapotranspiration. *Water Resources Research, 15*, 443-450

Garratt, J.R., & Hicks, B.B. (1973). Momentum, heat and water vapour transfer to and from natural and artificial surfaces. *Quarterly Journal of the Royal Meteorological Society, 99*, 680-687

Ghent, D., Veal, K., Trent, T., Dodd, E., Sembhi, H., & Remedios, J. (2019). A new approach to defining uncertainties for MODIS land surface temperature. *Remote Sensing, 11*, 1021

Grossiord, C., Buckley, T.N., Cernusak, L.A., Novick, K.A., Poulter, B., Siegwolf, R.T.W., Sperry, J.S., & McDowell, N.G. (2020). Plant responses to rising vapor pressure deficit. *New Phytologist, 226*, 1550-1566

Huband, N.D.S., & Monteith, J.L. (1986). Radiative surface temperature and energy balance of a wheat canopy. *Boundary-Layer Meteorology, 36*, 1-17

Kustas, W., & Anderson, M. (2009). Advances in thermal infrared remote sensing for land surface modeling. *Agricultural and Forest Meteorology, 149*, 2071-2081

Kustas, W.P., Anderson, M.C., Norman, J.M., & Li, F. (2007). Utility of radiometric–aerodynamic temperature relations for heat flux estimation. *Boundary-Layer Meteorology, 122*, 167-187

Lhomme, J.-P., Chehbouni, A., & Monteny, B. (2000). Sensible heat flux-radiometric surface temperature relationship over sparse vegetation: Parameterizing B-1. *Boundary-Layer Meteorology, 97*, 431-457

Lhomme, J. P., Troufleau, D., Monteny, B., Chehbouni, A., & Bauduin, S. (1997). Sensible heat flux and radiometric surface temperature over sparse Sahelian vegetation II. A model for the kb-1 parameter. *Journal of Hydrology*, 188, 839 – 854.

Li, Y., Kustas, W.P., Huang, C., Nieto, H., Haghighi, E., Anderson, M.C., Domingo, F., Garcia, M., & Scott, R.L. (2019). Evaluating soil resistance formulations in thermal-based two-source energy balance (TSEB) model: Implications for heterogeneous semiarid and arid regions. *Water Resources Research, 55*, 1059-1078

Lin, H., Chen, Y., Song, Q., Fu, P., Cleverly, J., Magliulo, V., Law, B.E., Gough, C.M., Hörtnagl, L., & Di Gennaro, F. (2017). Quantifying deforestation and forest degradation with thermal response. *Science of the Total Environment, 607*, 1286-1292

Mallick, K., Jarvis, A.J., Boegh, E., Fisher, J.B., Drewry, D.T., Tu, K.P., Hook, S.J., Hulley, G., Ardö, J., & Beringer, J. (2014). A Surface Temperature Initiated Closure (STIC) for surface energy balance fluxes. *Remote Sensing of Environment, 141*, 243-261

Mallick, K., Toivonen, E., Trebs, I., Boegh, E., Cleverly, J., Eamus, D., Koivusalo, H., Drewry, D., Arndt, S.K., & Griebel, A. (2018a). Bridging Thermal Infrared Sensing and Physically-Based Evapotranspiration Modeling: From Theoretical Implementation to Validation Across an Aridity Gradient in Australian Ecosystems. *Water Resources Research, 54*, 3409-3435

Mallick, K., Trebs, I., Boegh, E., Giustarini, L., Schlerf, M., Drewry, D.T., Hoffmann, L., Randow, C.v., Kruijt, B., & Araùjo, A. (2016). Canopy-scale biophysical controls of transpiration and evaporation in the Amazon Basin. *Hydrology and Earth System Sciences, 20*, 4237-4264

Mallick, K., Wandera, L., Bhattarai, N., Hostache, R., Kleniewska, M., & Chormanski, J. (2018b). A critical evaluation on the role of aerodynamic and canopy–surface conductance parameterization in SEB and SVAT models for simulating evapotranspiration: A case study in the upper biebrza national park wetland in poland. *Water, 10*, 1753

Massmann, A., Gentine, P., & Lin, C. (2019). When does vapor pressure deficit drive or reduce evapotranspiration? *Journal of advances in modeling earth systems, 11*, 3305-3320

Monteith, J.L. (1965). Evaporation and environment. In (pp. 205-234): Cambridge University Press (CUP) Cambridge

Priestley, C.H.B., & Taylor, R.J. (1972). On the assessment of surface heat flux and evaporation using large-scale parameters. *Monthly weather review, 100*, 81-92

Santanello Jr, J.A., & Friedl, M.A. (2003). Diurnal covariation in soil heat flux and net radiation. *Journal of Applied Meteorology, 42*, 851-862

Shuttleworth, W.J., Gurney, R.J., Hsu, A.Y., & Ormsby, J.P. (1989). FIFE: the variation in energy partition at surface flux sites. *IAHS Publ, 186*, 523-534

Trebs, I., Mallick, K., Bhattarai, N., Sulis, M., Cleverly, J., Woodgate, W., Silberstein, R., Hinko-Najera, N., Beringer, J., & Meyer, W.S. (2021). The role of aerodynamic resistance in thermal remote sensing-based evapotranspiration models. *Remote Sensing of Environment, 264*, 112602

Troufleau, D., Lhomme, J.-P., Monteny, B., & Vidal, A. (1997). Sensible heat flux and radiometric surface temperature over sparse Sahelian vegetation I. An experimental analysis of the kb-1 parameter. *Journal of Hydrology*, *188*, 815 – 838.

Venturini, V., Islam, S., & Rodriguez, L. (2008). Estimation of evaporative fraction and evapotranspiration from MODIS products using a complementary based model. *Remote Sensing of Environment, 112*, 132-141

Verhoef, A., De Bruin, H.A.R., & Van Den Hurk, B. (1997). Some practical notes on the parameter kB-1 for sparse vegetation, *Journal of Applied Meteorology*, *36*, 560 – 572.

Verma, S.B. (1989). Aerodynamic resistances to transfers of heat, mass and momentum. In, *Proceedings of a Workshop Held at Vancouver, B.C., Canada* (pp. 13-20): IAHS Publ

Wang, K., Wan, Z., Wang, P., Sparrow, M., Liu, J., Zhou, X., & Haginoya, S. (2005). Estimation of surface long wave radiation and broadband emissivity using Moderate Resolution Imaging Spectroradiometer (MODIS) land surface temperature/emissivity products. *Journal of Geophysical Research: Atmospheres, 110*